JACS
JOURNAL OF THE AMERICAN CHEMICAL SOCIETY
pubs.acs.org/JACS
Communication

Isolated Cobalt Centers on $W_{18}O_{49}$ Nanowires Perform as a Reaction Switch for Efficient CO_2 Photoreduction

Huabin Zhang, Yan Wang, Shouwei Zuo, Wei Zhou, Jing Zhang, and Xiong Wen David Lou*

Cite This: J. Am. Chem. Soc. 2021, 143, 2173–2177
Read Online

ABSTRACT: Isolated cobalt atoms have been successfully decorated onto the surface of $W_{18}O_{49}$ ultrathin nanowires. The Co-atom-decorated $W_{18}O_{49}$ nanowires ($W_{18}O_{49}$@Co) greatly accelerate the charge carrier separation and electron transport in the catalytic system. Moreover, the surface decoration with Co atoms modifies the energy configuration of the $W_{18}O_{49}$@Co hybrid and thus boosts the redox capability of photoexcited electrons for CO_2 reduction. The decorated Co atoms work as the real active sites and, perhaps more importantly, perform as a reaction switch to enable the reaction to proceed. The optimized catalyst delivers considerable activity for photocatalytic CO_2 reduction, yielding an impressive CO generation rate of 21.18 mmol g^{-1} h^{-1}.

Converting CO_2 into chemical products and renewable energy via artificial photosynthesis is an ideal strategy to simultaneously alleviate the escalating energy shortages and climate changes.[1−4] However, as of today, the energy efficiency of solar-driven CO_2 conversion is still limited, which should be attributed to the high chemical inertness of linear CO_2 molecules and the fast recombination of photogenerated charge carriers.[5−9] The separation/transfer efficiencies of the photogenerated electron−hole pairs and the energy band configuration of the catalytic system are of vital importance in determining the redox potentials.[10−12] Thus, modulating the band gap energies between the electron donors and acceptors as well as surface energies of the cocatalyst should be effective in improving the photocatalytic efficiency.[13,14]

One holy grail in the synthesis of catalysts is to construct hybrids with the designed electronic structure and catalytic performance through, for example, controllable manipulation of metal atoms.[15,16] Single-atom catalysts with the maximum atomic utilization efficiency often give impressive activity in heterogeneous catalysis.[17−19] Furthermore, atomic modification has also offered an opportunity to regulate the redox capability of excited electrons and holes in the catalytic process.[20] Nevertheless, single-atomic modification for switching the reaction route is still in the early stage and has not yet been systematically developed.

Herein, we realize the decoration of isolated Co atoms onto $W_{18}O_{49}$ ultrathin nanowires (designated as $W_{18}O_{49}$@Co) through surface modification engineering. X-ray absorption fine structure spectroscopy verifies that the decorated Co atoms are confined in the surface lattice of $W_{18}O_{49}$ ultrathin nanowires. Experimental results and density functional theory (DFT) calculations reveal that the isolated Co atoms not only perform as the active centers for the CO_2 reduction but also greatly modify the energy band configuration of the hybrid. The negatively shifted flat band in Co-decorated $W_{18}O_{49}$ ultrathin nanowires fundamentally changes its CO_2 reduction capability, resulting in highly accelerated catalytic kinetics and promoted photocatalytic efficiency.

The synthetic approach for $W_{18}O_{49}$@Co is shown in Figure 1a. First, a facile method has been employed to synthesize

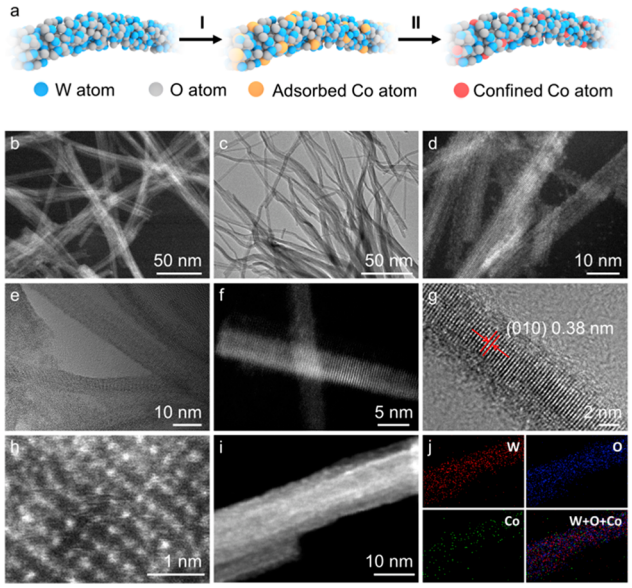

Figure 1. (a) Schematic of the synthetic process for the $W_{18}O_{49}$@Co hybrid: (I) decoration of Co species and (II) thermal annealing in air. (b−f) STEM (b, d, and f) and TEM images (c and e) of the $W_{18}O_{49}$@Co nanowires. (g) HRTEM image of one $W_{18}O_{49}$@Co nanowire. (h) Atomic resolution ADF-STEM image of $W_{18}O_{49}$@Co. (i, j) HAADF-STEM image of $W_{18}O_{49}$@Co (i) and related elemental mapping images (j).

Received: August 11, 2020
Published: January 28, 2021

https://dx.doi.org/10.1021/jacs.0c08409
J. Am. Chem. Soc. 2021, 143, 2173−2177

$W_{18}O_{49}$ nanowires.[21] Transmission electron microscopy (TEM) and scanning transmission electron microscopy (STEM) investigations confirm that the one-dimensional nanowires are uniform in diameter (Figure S1). Subsequently, the Co species is further loaded on the as-synthesized $W_{18}O_{49}$ nanowires by mixing with $Co(NO_3)_2$ in an ethanol solution at room temperature. Calcination of the Co-loaded sample at a high temperature in air is conducted to enhance the mutual interaction between the decorated Co atoms and $W_{18}O_{49}$ nanowires.

STEM and TEM images confirm that the one-dimensional morphology is well maintained in $W_{18}O_{49}$@Co (Figure 1b–f). The X-ray diffraction (XRD) patterns of $W_{18}O_{49}$ and $W_{18}O_{49}$@Co are quite similar, which are both indexed as monoclinic $W_{18}O_{49}$ (JCPDS card No. 71-2450) (Figure S2).[22] A high-resolution TEM (HRTEM) image verifies the ordered lattice fringes with an interplanar distance of 3.8 Å, which can be indexed to the (010) plane of monoclinic $W_{18}O_{49}$ (Figure 1g). These results also indicate that there is no change in the crystal phase after the Co decoration. To further determine the atomic structure, annular dark-field (ADF) imaging has been conducted on an aberration-corrected STEM system. An ADF image represents the projection of atoms along the incident beam direction. Therefore, a high-resolution aberration-corrected ADF-STEM image of $W_{18}O_{49}$@Co is used to characterize the dispersion and configuration of the Co and W atoms on the basis of the *Z*-difference of the individual heavy atoms (Figure 1h). The confinement of the isolated Co atoms within the surface lattice of $W_{18}O_{49}$@Co has been clearly demonstrated without obvious Co atom aggregations. Energy-dispersive X-ray (EDX) and X-ray photoelectron spectroscopy (XPS) analyses confirm the successful decoration of Co species over the $W_{18}O_{49}$ nanowires (Figures S3 and S4). The high-angle annular dark-field STEM (HAADF-STEM) image and the EDX elemental mapping images reveal the even distribution of the Co element throughout the whole nanowires (Figure 1i,j). Gas adsorption investigations further confirm the existence of interparticle mesopores in the as-synthesized hybrids (Figures S5 and S6).

The Fourier transform of Co K-edge extended X-ray absorption fine structure (EXAFS) of $W_{18}O_{49}$@Co shows a dominating Co–O peak at 1.51 Å, which nearly overlays with the Co–O peak at 1.39 Å of the Co_3O_4 (Figure 2a).[23] Besides, no signal for Co–Co/Co–O–Co bonding is observed in $W_{18}O_{49}$@Co, confirming that the decorated Co atoms should be isolated without any aggregation in the form of Co/CoO_x particles or clusters (Figure S7).[24] Quantitative EXAFS curve-fitting analyses for $W_{18}O_{49}$@Co verify that the average coordination number for the isolated Co sites in the first coordination sphere is 5.6 with the bond length of 2.06 Å, while the coordination number for the Co–W interaction in the second coordination sphere is 5.5 at the distance of 3.35 Å (Figure 2b,d, Figures S8 and S9, and Table S1). These results demonstrate that the coordination sphere of Co sites in $W_{18}O_{49}$@Co is slightly distorted in an unsaturated configuration, and they also verify that the Co atoms are confined in the lattice of $W_{18}O_{49}$, with the Co–W interaction in the second coordination sphere. Wavelet transform (WT) analyses offer a higher resolution in the radial distance. The WT intensity maxima near 4.0 and 3.9 $Å^{-1}$ that arise from the light atom coordination are well detected for $W_{18}O_{49}$@Co and Co_3O_4, respectively. Nevertheless, an intensity maximum at about 6.6 $Å^{-1}$, associated with the Co–Co bonding in Co foil, is not observed in $W_{18}O_{49}$@Co (Figure 2c). The obvious differences in X-ray absorption near-edge structure (XANES) profiles between the $W_{18}O_{49}$@Co and Co foil also exclude the existence of Co–Co coordination in $W_{18}O_{49}$@Co (Figure 2e).[25] The white line peak intensity of $W_{18}O_{49}$@Co is slightly stronger than those of Co_3O_4 and Co_2O_3. Linear fitting for the absorption edges of XANES curves confirms that the average oxidation state of Co species in $W_{18}O_{49}$@Co should be 3.3 (Figure S10).[26,27]

The photocatalytic CO_2 reduction performance is evaluated in a tandem system with the optimized catalyst dosage, while $[Ru(bpy)_3]Cl_2·6H_2O$ (abbreviated as **Ru**, bpy = 2,2′-bipyridine) is applied as the photosensitizer (Figure S11).[26] In this reaction system, only CO and H_2 are generated, and no appreciable amounts of other products are detected (Figures S12 and S13). The effect of loading amounts of Co component is first investigated, and the hybrid with the loading amount of 1.4 wt% gives the highest activity and selectivity for the CO_2-to-CO conversion reaction (Figure S14). As observed from the time–yield plots, the optimized $W_{18}O_{49}$@Co hybrid exhibits an impressive CO generation rate of 21.18 mmol g^{-1} h^{-1} and a H_2 generation rate of 6.49 mmol g^{-1} h^{-1} for the first hour (Figure 3a). The CO evolution rate of $W_{18}O_{49}$@Co compares favorably to those of catalysts reported recently (Table S2). It is notable that the product evolution rates gradually decrease in the catalytic process. This phenomenon is commonly observed and

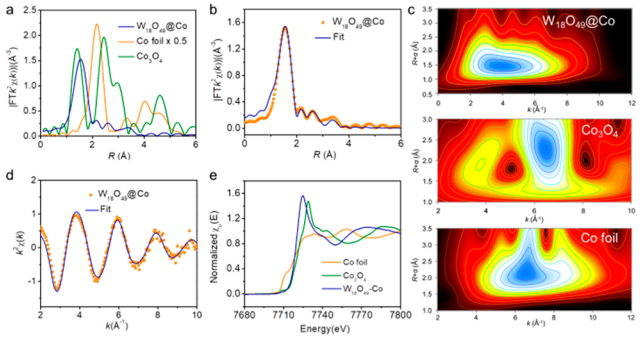

Figure 2. (a) Fourier-transformed magnitudes of the experimental Co K-edge EXAFS spectra. Fourier-transformed magnitudes of Co K-edge EXAFS spectra in (b) *R* space and (d) *K* space for $W_{18}O_{49}$@Co. (c) WT for the k^3-weighted EXAFS signal. (e) Co K-edge XANES experimental spectra.

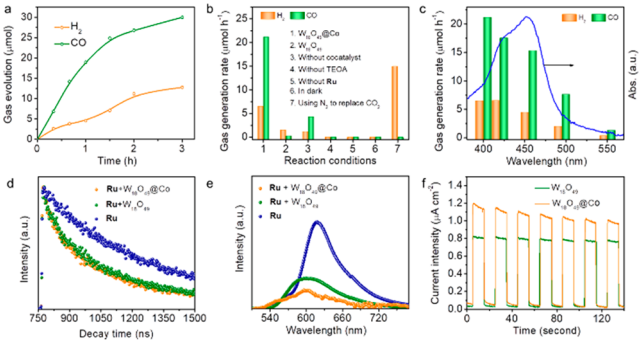

Figure 3. (a) Time-dependent CO and H_2 evolution of $W_{18}O_{49}$@Co. (b) Gas generation rates in the catalytic system under different reaction conditions. (c) Wavelength-dependent gas generation rates of $W_{18}O_{49}$@Co, and the light absorption spectrum of the **Ru** photosensitizer. (d) TRPL spectra. (e) Steady-state PL spectra. (f) Transient photocurrent responses of $W_{18}O_{49}$ and $W_{18}O_{49}$@Co.

https://dx.doi.org/10.1021/jacs.0c08409
J. Am. Chem. Soc. 2021, 143, 2173–2177

should be ascribed to the degradation of the **Ru** photosensitizer.[28−30] It should be noted that the catalytic performance of $W_{18}O_{49}$ without decoration of Co atoms is rather poor and nearly undetectable (Figure S15). These results clearly demonstrate that the decorated Co atoms perform as a reaction switch to enable the catalysis process to proceed. The $W_{18}O_{49}$@Co hybrid also shows high durability in cycling tests and presents reasonably reproducible photocatalytic activity in each cycle (Figure S16). Moreover, the $W_{18}O_{49}$@Co hybrid has been characterized thoroughly after the catalytic process. There is no obvious structural evolution or loss of the Co content for the catalyst in the reaction process, further revealing its high stability in the CO_2 reduction process (Figure S17).

Control experiments are conducted to further understand the CO_2 reduction under various conditions (Figure 3b). No CO or H_2 is detected without the addition of triethanolamine (TEOA) to the reaction system, confirming that TEOA is indispensable in the CO_2 reduction process. This result is also consistent with previous reports.[31,32] The CO_2 reduction process is also investigated in the absence of visible light, and the whole reaction is immediately terminated. This result verifies that the CO_2 reduction is indeed driven by the photoirradiation. When N_2 is used as the feedstock gas instead of CO_2, no CO gas is detected from the catalytic process, suggesting that the generated CO product should originate from the CO_2 reactant. To provide direct proof for the carbon source of evolved CO, ^{13}C-isotopic tracer experiments are carried out. Results of the gas chromatography−mass spectrometry analysis reveal that only ^{13}CO is detected when $^{13}CO_2$ is used as the gas source, clearly demonstrating that the produced CO is originated from photocatalytic reduction of CO_2 molecules (Figure S18). In the absence of the **Ru** photosensitizer, nearly no product gas is detected. Besides, wavelength-dependent CO/H_2 evolutions have also been investigated. The product generation rates qualitatively follow the characteristic absorption spectrum of the **Ru** photosensitizer (Figure 3c).[10,33] These results confirm that the CO_2 reduction reaction is indeed triggered by light excitation of the **Ru** photosensitizer.

Time-resolved photoluminescence (TRPL) spectroscopy is applied to monitor the charge carrier dynamics (Figure 3d). The decay kinetics of $W_{18}O_{49}$@Co/**Ru** displays a shorter average lifetime (450.3 ns) than those of $W_{18}O_{49}$/**Ru** (459.9 ns) and **Ru** (846.1 ns), confirming that the former can greatly enhance the separation of photogenerated charge carriers (Figure S19 and Table S3).[5,31] Moreover, photoluminescence (PL) spectroscopy has been applied to probe the recombination of light-excited charge carriers. As observed, $W_{18}O_{49}$@Co/**Ru** greatly prohibits the recombination of electrons and holes in the excitation process (Figure 3e). Greatly enhanced photocurrent intensity and reduced charge-transfer resistance have been observed over the $W_{18}O_{49}$@Co hybrid (Figure 3f and Figure S20).[10,29] These results confirm the positive effects of Co decoration in the separation of photogenerated charge carriers and also suggest that the isolated Co atoms can serve as the electron pump and promote the charge separation and transport efficiency.

In photocatalysis, one key factor that determines the photocatalytic capability of a catalyst is its electronic structure.[2] The impact of Co atom decoration on the electronic structure of $W_{18}O_{49}$ is first examined, as the Co atom possesses a different electronic structure and electronegativity compared to the W atom. Mott−Schottky plot analysis is a powerful method to determine the flat-band position. For the n-type semiconductor, the conduction band (CB) position is about 0.3 V lower than the flat-band position. Thus, we can further confirm the value of CB via the Mott−Schottky plot. The CB potential for $W_{18}O_{49}$ is confirmed as 0.13 V versus normal hydrogen electrode (NHE, pH = 0), which is insufficient to drive the CO_2-to-CO reduction process (Figure 4a).[34−36] This result also explains the early

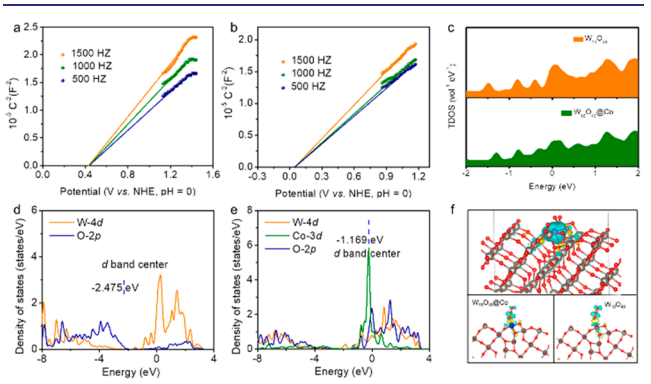

Figure 4. Mott−Schottky plots of (a) $W_{18}O_{49}$ and (b) $W_{18}O_{49}$@Co. (c) Calculated TDOS of $W_{18}O_{49}$@Co and $W_{18}O_{49}$. Calculated PDOS of (d) $W_{18}O_{49}$@Co and (e) $W_{18}O_{49}$. (f) Calculated differential charge density for $W_{18}O_{49}$@Co (upper) and CO_2 molecule adsorbed structural models (lower).

observation that the CO evolution over $W_{18}O_{49}$ is nearly undetectable. The energy band configuration of $W_{18}O_{49}$ is greatly modified after the decoration of Co atoms (Figure 4b). A negatively shifted CB potential of −0.25 V is observed in $W_{18}O_{49}$@Co, which is more negative than the reduction potential of CO_2/CO (−0.105 V). These results clearly verify that the Co atom decoration greatly improves the redox capability of photoexcited electrons. Besides, the redox potential of $Ru(bpy)_3^{2+}/Ru(bpy)_3^{+}$ (−0.68 V vs NHE) is more negative than the flat-band potential of the $W_{18}O_{49}$@Co hybrid.[2] These results suggest that the $W_{18}O_{49}$@Co catalyst is thermodynamically capable of receiving the photoexcited electrons from the excited **Ru** photosensitizer for reducing the adsorbed CO_2 to CO product (Figure S21). It might thus be concluded that the modulated CB position of $W_{18}O_{49}$@Co endows sufficient driving force to trigger the CO_2 reduction to proceed.

The DFT calculations clearly confirm that the Co decoration results in some new impurity levels in the total density of state (TDOS), which is favorable for excitation of electrons into the CB, thus guaranteeing higher photoconversion efficiency (Figure 4c, Figures S22 and S23). The projected density of state (PDOS) calculations reveal that the most prominent characteristic in $W_{18}O_{49}$@Co is the emergence of a free-atom-like d-band center, in sharp contrast to the broader d-band of the $W_{18}O_{49}$ without Co decoration (Figure 4d,e).[37,38] According to the Kohn−Sham orbitals for the new bands near the Fermi level, these states, localized around the isolated Co sites, can perform as the reaction switch for controlling the proceeding of the reaction.[39] Moreover, the upshifting of the d-band center from −2.475 to −1.169 eV is also observed after the Co atom decoration. It is well established that the upshifted d-band center can push more antibonding states above the Fermi level, thus resulting in decreased occupation and stronger adsorbate bonding.[40] The Co atom decoration shifts the d-band center closer to the Fermi level and results in stronger surface bonding with the CO_2 molecules. As confirmed by the differential charge densities over the CO_2-adsorbed structural models, higher concentrations of electrons are transferred to the near-surface

https://dx.doi.org/10.1021/jacs.0c08409
J. Am. Chem. Soc. 2021, 143, 2173−2177

region of $W_{18}O_{49}$@Co (Figure 4f). This result is also consistent with the experimentally measured CO_2 adsorption capacities (Figure S6). Therefore, the greatly elevated d-band center of $W_{18}O_{49}$@Co would further boost the catalytic activity of Co sites.

In summary, $W_{18}O_{49}$ nanowires decorated with isolated Co atoms have been developed as an efficient catalyst for CO_2 photoreduction. The decorated Co atoms not only perform as the active centers for CO_2 reduction but also work as the reaction switch for the reaction to proceed. Experimental results confirm that the energy band configuration of $W_{18}O_{49}$ is greatly modified after the decoration of Co atoms, which results in a negatively shifted flat-band potential and greatly improved redox capability. DFT calculations further reveal that the free-atom-like d-band center should be fundamentally responsible for the change in redox capability. The current work develops an excellent catalyst for CO_2 reduction and, more importantly, provides some inspiration for effectively modulating the electronic structure and catalytic performance of the catalysts for various photoreduction processes.

■ ASSOCIATED CONTENT

Supporting Information

The Supporting Information is available free of charge at https://pubs.acs.org/doi/10.1021/jacs.0c08409.

Experimental details, more FESEM/TEM images, and XRD, EDX, XPS, and EXAFS plots (PDF)

■ AUTHOR INFORMATION

Corresponding Author

Xiong Wen David Lou − *School of Chemical and Biomedical Engineering, Nanyang Technological University, Singapore 637459, Singapore;* orcid.org/0000-0002-5557-4437; Email: xwlou@ntu.edu.sg

Authors

Huabin Zhang − *School of Chemical and Biomedical Engineering, Nanyang Technological University, Singapore 637459, Singapore;* orcid.org/0000-0003-1601-2471

Yan Wang − *School of Chemical and Biomedical Engineering, Nanyang Technological University, Singapore 637459, Singapore*

Shouwei Zuo − *Beijing Synchrotron Radiation Facility, Institute of High Energy Physics, Chinese Academy of Sciences, Beijing 100049, China*

Wei Zhou − *Department of Applied Physics, Faculty of Science, Tianjin University, Tianjin 300072, P. R. China;* orcid.org/0000-0002-8004-3996

Jing Zhang − *Beijing Synchrotron Radiation Facility, Institute of High Energy Physics, Chinese Academy of Sciences, Beijing 100049, China;* orcid.org/0000-0002-3750-374X

Complete contact information is available at: https://pubs.acs.org/10.1021/jacs.0c08409

Notes

The authors declare no competing financial interest.

■ ACKNOWLEDGMENTS

X.W.L. acknowledges the funding support from the Ministry of Education of Singapore through the Academic Research Fund (AcRF) Tier-2 grant (MOE2017-T2-2-003) and Tier-1 grant (RG116/18).

■ REFERENCES

(1) Jiang, Z.; Sun, H.; Wang, T.; Wang, B.; Wei, W.; Li, H.; Yuan, S.; An, T.; Zhao, H.; Yu, J.; Wong, P. K. Nature-Based Catalyst for Visible-Light-Driven Photocatalytic CO_2 Reduction. *Energy Environ. Sci.* **2018**, *11*, 2382−2389.

(2) Tong, H.; Ouyang, S.; Bi, Y.; Umezawa, N.; Oshikiri, M.; Ye, J. Nano-Photocatalytic Materials: Possibilities and Challenges. *Adv. Mater.* **2012**, *24*, 229−251.

(3) Mateo, D.; Albero, J.; García, H. Titanium-Perovskite-Supported RuO_2 Nanoparticles for Photocatalytic CO_2 Methanation. *Joule* **2019**, *3*, 1949−1962.

(4) Ran, J.; Jaroniec, M.; Qiao, S. Z. Cocatalysts in Semiconductor Based Photocatalytic CO_2 Reduction: Achievements, Challenges, and Opportunities. *Adv. Mater.* **2018**, *30*, 1704649.

(5) Jiang, Z.; Wan, W.; Li, H.; Yuan, S.; Zhao, H.; Wong, P. K. A Hierarchical Z-Scheme α-Fe_2O_3/g-C_3N_4 Hybrid for Enhanced Photocatalytic CO_2 Reduction. *Adv. Mater.* **2018**, *30*, 1706108.

(6) Xu, Y. F.; Yang, M. Z.; Chen, B. X.; Wang, X. D.; Chen, H. Y.; Kuang, D. B.; Su, C. Y. A $CsPbBr_3$ Perovskite Quantum Dot/Graphene Oxide Composite for Photocatalytic CO_2 Reduction. *J. Am. Chem. Soc.* **2017**, *139*, 5660−5663.

(7) Zhang, H.; Wang, T.; Wang, J.; Liu, H.; Dao, T. D.; Li, M.; Liu, G.; Meng, X.; Chang, K.; Shi, L.; Nagao, T.; Ye, J. Surface-Plasmon-Enhanced Photodriven CO_2 Reduction Catalyzed by Metal-Organic-Framework-Derived Iron Nanoparticles Encapsulated by Ultrathin Carbon Layers. *Adv. Mater.* **2016**, *28*, 3703−3710.

(8) Xu, G.; Zhang, H.; Wei, J.; Zhang, H. X.; Wu, X.; Li, Y.; Li, C.; Zhang, J.; Ye, J. Integrating the g-C_3N_4 Nanosheet with B-H Bonding Decorated Metal-Organic Framework for CO_2 Activation and Photoreduction. *ACS Nano* **2018**, *12*, 5333−5340.

(9) Zhang, H.; Liu, G.; Shi, L.; Liu, H.; Wang, T.; Ye, J. Engineering Coordination Polymers for Photocatalysis. *Nano Energy* **2016**, *22*, 149−168.

(10) Zhang, H.; Zhang, P.; Qiu, M.; Dong, J.; Zhang, Y.; Lou, X. W. Ultrasmall MoO_x Clusters as a Novel Cocatalyst for Photocatalytic Hydrogen Evolution. *Adv. Mater.* **2019**, *31*, 1804883.

(11) Hisatomi, T.; Domen, K. Reaction Systems for Solar Hydrogen Production via Water Splitting with Particulate Semiconductor Photocatalysts. *Nat. Catal.* **2019**, *2*, 387−399.

(12) Zhang, H.; Zuo, S.; Qiu, M.; Wang, S.; Zhang, Y.; Zhang, J.; Lou, X. W. Direct Probing of Atomically Dispersed Ru Species over Multi-edged TiO_2 for Highly Efficient Photocatalytic Hydrogen Evolution. *Sci. Adv.* **2020**, *6*, eabb9823.

(13) Zhang, N.; Jalil, A.; Wu, D.; Chen, S.; Liu, Y.; Gao, C.; Ye, W.; Qi, Z.; Ju, H.; Wang, C.; Wu, X.; Song, L.; Zhu, J.; Xiong, Y. Refining Defect States in $W_{18}O_{49}$ by Mo Doping: a Strategy for Tuning N_2 Activation Towards Solar-Driven Nitrogen Fixation. *J. Am. Chem. Soc.* **2018**, *140*, 9434−9443.

(14) Tong, Y.; Guo, H.; Liu, D.; Yan, X.; Su, P.; Liang, J.; Zhou, S.; Liu, J.; Lu, G. Q.; Dou, S. X. Vacancy Engineering of Iron-Doped $W_{18}O_{49}$ Nanoreactors for Low-Barrier Electrochemical Nitrogen Reduction. *Angew. Chem., Int. Ed.* **2020**, *59*, 7356−7361.

(15) Ji, S.; Chen, Y.; Wang, X.; Zhang, Z.; Wang, D.; Li, Y. Chemical Synthesis of Single Atomic Site Catalysts. *Chem. Rev.* **2020**, *120*, 11900−11955.

(16) Ziatdinov, M.; Dyck, O.; Li, X.; Sumpter, B. G.; Jesse, S.; Vasudevan, R. K.; Kalinin, S. V. Building and Exploring Libraries of Atomic Defects in Graphene: Scanning Transmission Electron and Scanning Tunneling Microscopy Study. *Sci. Adv.* **2019**, *5*, eaaw8989.

(17) Zhang, H.; Lu, X. F.; Wu, Z.-P.; Lou, X. W. Emerging Multifunctional Single-Atom Catalysts/Nanozymes. *ACS Cent. Sci.* **2020**, *6*, 1288−1301.

(18) Zhang, H.; Liu, Y.; Chen, T.; Zhang, J.; Zhang, J.; Lou, X. W. Unveiling the Activity Origin of Electrocatalytic Oxygen Evolution over Isolated Ni Atoms Supported on a N-Doped Carbon Matrix. *Adv. Mater.* **2019**, *31*, 1904548.

(19) Zhang, H.; Zhou, W.; Lu, X. F.; Chen, T.; Lou, X. W. Implanting Isolated Ru Atoms into Edge-Rich Carbon Matrix for Efficient

Electrocatalytic Hydrogen Evolution. *Adv. Energy Mater.* **2020**, *10*, 2000882.
(20) Wang, C.; Li, A.; Li, C.; Zhang, S.; Li, H.; Zhou, X.; Hu, L.; Feng, Y.; Wang, K.; Zhu, Z.; et al. Ultrahigh Photocatalytic Rate at a Single-Metal-Atom-Oxide. *Adv. Mater.* **2019**, *31*, 1903491.
(21) Xi, G.; Ouyang, S.; Li, P.; Ye, J.; Ma, Q.; Su, N.; Bai, H.; Wang, C. Ultrathin $W_{18}O_{49}$ Nanowires with Diameters Below 1 nm: Synthesis, Near-Infrared Absorption, Photoluminescence, and Photochemical Reduction of Carbon Dioxide. *Angew. Chem., Int. Ed.* **2012**, *51*, 2395−2399.
(22) Cong, S.; Yuan, Y.; Chen, Z.; Hou, J.; Yang, M.; Su, Y.; Zhang, Y.; Li, L.; Li, Q.; Geng, F.; Zhao, Z. Noble Metal-Comparable SERS Enhancement from Semiconducting Metal Oxides by Making Oxygen Vacancies. *Nat. Commun.* **2015**, *6*, 7800.
(23) Tahir, M.; Pan, L.; Zhang, R.; Wang, Y.-C.; Shen, G.; Aslam, I.; Qadeer, M. A.; Mahmood, N.; Xu, W.; Wang, L.; Zhang, X.; Zou, J.-J. High-Valence-State NiO/Co_3O_4 Nanoparticles on Nitrogen-Doped Carbon for Oxygen Evolution at Low Overpotential. *ACS Energy Lett.* **2017**, *2*, 2177−2182.
(24) Zhang, H.; Zhou, W.; Dong, J.; Lu, X. F.; Lou, X. W. Intramolecular Electronic Coupling in Porous Iron Cobalt (oxy) Phosphide Nanoboxes Enhances the Electrocatalytic Activity for Oxygen Evolution. *Energy Environ. Sci.* **2019**, *12*, 3348−3355.
(25) Maeda, K.; Ishimaki, K.; Okazaki, M.; Kanazawa, T.; Lu, D.; Nozawa, S.; Kato, H.; Kakihana, M. Cobalt Oxide Nanoclusters on Rutile Titania as Bifunctional Units for Water Oxidation Catalysis and Visible Light Absorption: Understanding the Structure-Activity Relationship. *ACS Appl. Mater. Interfaces* **2017**, *9*, 6114−6122.
(26) Wang, H.-Y.; Hung, S.-F.; Chen, H.-Y.; Chan, T.-S.; Chen, H. M.; Liu, B. In Operando Identification of Geometrical-Site-Dependent Water Oxidation Activity of Spinel Co_3O_4. *J. Am. Chem. Soc.* **2016**, *138*, 36−39.
(27) Zandkarimi, B.; Sun, G.; Halder, A.; Seifert, S.; Vajda, S.; Sautet, P.; Alexandrova, A. N. Interpreting the Operando XANES of Surface-Supported Subnanometer Clusters: When Fluxionality, Oxidation State, and Size Effect Fight. *J. Phys. Chem. C* **2020**, *124*, 10057−10066.
(28) Lewis, N. S.; Nocera, D. G. Powering the Planet: Chemical Challenges in Solar Energy Utilization. *Proc. Natl. Acad. Sci. U. S. A.* **2006**, *103*, 15729−15735.
(29) Listorti, A.; Durrant, J.; Barber, J. Solar to Fuel. *Nat. Mater.* **2009**, *8*, 929−930.
(30) Brethomé, F. M.; Williams, N. J.; Seipp, C. A.; Kidder, M. K.; Custelcean, R. Direct Air Capture of CO_2 via Aqueous-Phase Absorption and Crystalline-Phase Release using Concentrated Solar Power. *Nat. Energy* **2018**, *3*, 553−559.
(31) Gao, C.; Meng, Q.; Zhao, K.; Yin, H.; Wang, D.; Guo, J.; Zhao, S.; Chang, L.; He, M.; Li, Q.; et al. Co_3O_4 Hexagonal Platelets with Controllable Facets Enabling Highly Efficient Visible-Light Photocatalytic Reduction of CO_2. *Adv. Mater.* **2016**, *28*, 6485−6490.
(32) Wang, Y.; Wang, S.; Lou, X. W. Dispersed Nickel Cobalt Oxyphosphide Nanoparticles Confined in Multichannel Hollow Carbon Fibers for Photocatalytic CO_2 Reduction. *Angew. Chem., Int. Ed.* **2019**, *58*, 17236−17240.
(33) Niu, K.; Xu, Y.; Wang, H.; Ye, R.; Xin, H. L.; Lin, F.; Tian, C.; Lum, Y.; Bustillo, K. C.; Doeff, M. M.; et al. A Spongy Nickel-Organic CO_2 Reduction Photocatalyst for Nearly 100% Selective CO Production. *Sci. Adv.* **2017**, *3*, e1700921.
(34) Shi, L.; Wang, T.; Zhang, H.; Chang, K.; Meng, X.; Liu, H.; Ye, J. An Amine-Functionalized Iron (III) Metal-Organic Framework as Efficient Visible-Light Photocatalyst for Cr (VI) Reduction. *Adv. Sci.* **2015**, *2*, 1500006.
(35) Zhang, Z.; Jiang, X.; Liu, B.; Guo, L.; Lu, N.; Wang, L.; Huang, J.; Liu, K.; Dong, B. IR-Driven Ultrafast Transfer of Plasmonic Hot Electrons in Nonmetallic Branched Heterostructures for Enhanced H_2 Generation. *Adv. Mater.* **2018**, *30*, 1705221.
(36) Zhang, Z.; Huang, J.; Fang, Y.; Zhang, M.; Liu, K.; Dong, B. A Nonmetal Plasmonic Z-scheme Photocatalyst with UV-to NIR-Driven Photocatalytic Protons Reduction. *Adv. Mater.* **2017**, *29*, 1606688.
(37) Zhao, Z.; Lu, G. Cu-based Single-Atom Catalysts Boost Electroreduction of CO_2 to CH_3OH: First-Principles Predictions. *J. Phys. Chem. C* **2019**, *123*, 4380−4387.
(38) Li, Y.; Zhang, R.; Zhou, W.; Wu, X.; Zhang, H.; Zhang, J. Hierarchical MoS_2 Hollow Architectures with Abundant Mo Vacancies for Efficient Sodium Storage. *ACS Nano* **2019**, *13*, 5533−5540.
(39) Zhang, H.; Yu, L.; Chen, T.; Zhou, W.; Lou, X. W. Surface Modulation of Hierarchical MoS_2 Nanosheets by Ni Single Atoms for Enhanced Electrocatalytic Hydrogen Evolution. *Adv. Funct. Mater.* **2018**, *28*, 1807086.
(40) Darby, M. T.; Réocreux, R.; Sykes, E. C. H.; Michaelides, A.; Stamatakis, M. Elucidating the Stability and Reactivity of Surface Intermediates on Single-Atom Alloy Catalysts. *ACS Catal.* **2018**, *8*, 5038−5050.

https://dx.doi.org/10.1021/jacs.0c08409
J. Am. Chem. Soc. 2021, 143, 2173−2177